A generic numerical solver for modeling the influence of stress conditions on guided wave propagation for SHM applications.

Andre Dalmora, Alexandre Imperiale, Sébastien Imperiale, Philippe Moireau

Proceedings of the ASME 2022
49th Annual Review of Progress in
Quantitative Nondestructive Evaluation
QNDE2022
July 25-27, 2022, San Diego, CA

QNDE2022-98682

A GENERIC NUMERICAL SOLVER FOR MODELING THE INFLUENCE OF STRESS CONDITIONS ON GUIDED WAVE PROPAGATION FOR SHM APPLICATIONS

André Dalmora[1,2,3,*], Alexandre Imperiale[1], Sébastien Imperiale[2,3], Philippe Moireau[2,3]

[1]Université Paris-Saclay, CEA, List, F-91120, Palaiseau, France
[2]Inria, Project-Team MΞDISIM, Inria Saclay-Île-de-France, 91128 Palaiseau, France
[2]LMS, Ecole Polytechnique, CNRS, Institut Polytechnique de Paris, 91128 Palaiseau, France

ABSTRACT

In leading-edge industrial applications, assessing structure integrity is an important aspect of safety requirements. Structural Health Monitoring (SHM) proposes to use sensors and signal processing units in situ. One of the most attractive SHM techniques relies on ultrasonic guided waves. Modeling and simulation can be helpful tools for the design or the reliability assessment of SHM solutions. Currently available models developed for that purpose do not take into account effects of operational conditions such as internal stresses. These conditions can change wave propagation and therefore affect the interpretation of recorded signals. The objective of this work is to propose a model that fills this gap, and to derive corresponding numerical methods for elastic wave propagation in an arbitrarily deformed medium. Any hyperelastic constitutive law can be considered. As the structures considered are usually thin, we avoid shear-locking by using a shell formulation to solve the quasi-static problem representing the effects of structure loading. The computed displacement is then fed into a spectral elements method (SFEM) kernel to solve the time-domain linearized 3D elastodynamics problem representing the wave propagation. We validate our model against experimental data in the literature for an isotropic aluminium plate under tensile forces. Additionally, we apply these numerical procedures to a realistic bending experiment of a steel pipe. These validations steps show that our generic approach is able to capture the effects of stresses on ultrasonic guided wave propagation such as changes in wave velocity and induced anisotropy.

Keywords: Numerical Simulation, Wave Propagation, Structural Health Monitoring, EOCs, Prestresses, Guided Waves, 3D Shell Elements, Spectral Finite Elements

*Corresponding author: andre.dalmora@cea.fr

1. INTRODUCTION

Assessing the operational state and lifetime of structures is of increasing importance and the demands for inspection are increasing as they age. Such need to assure their well-functioning fostered the development of advanced Non-Destructive Testing (NDT) techniques and Structural Health Monitoring (SHM) systems. SHM systems propose to use sensors and signal processing units *in situ*, aiming at a continuous assessment of the structural integrity among other monitoring capabilities. Ultrasonic Guided Waves (GW) is one of the means employed for implementing such systems [1, 2]. GW has the advantage of propagating over long distances and interacting with inhomogeneities and defects, transporting information about the medium.

Nonetheless, GW propagation is known to be influenced by Environmental and Operational conditions (EOCs) [3], posing a difficulty when the objective is to assure predictability of SHM systems. One type of operational condition of specific interest in this communication is structural loading. Structural loading originates from mechanical solicitations sustained by the structure during its use. It results in deformations and internal stresses that affect GW propagation. If not taken into account, these prestresses can significantly decrease SHM systems' capability to detect an anomaly. Although signal differentiation and baseline subtraction are proposed to overcome it [4], these techniques are less efficient for complex deformations and prestress profiles. This motivates the need for accurate modeling of EOCs perturbations on the system observations to increase SHM systems' robustness.

In the literature, various works can be found on modeling wave propagation in prestressed media. Most of them make use of Semi-Analytical methods to solve eigenproblems that output eigenmodes for GW given a specific stress profile. For instance, Treyssède worked on modeling guided wave propagation in helical wire strands [5] subjected to tensile forces. Loveday and

Wilcox uses the effects on GW of axial load in rails [6] to retrieve the axial load using GW. They considered the isotropic case with uniaxial forces. Shi et al. use the stress-induced anisotropy on isotropic plates to retrieve constants that characterizes the change in Lamb waves velocity due to external loads [7]. Wu et al. present an extension of the semi-analytical method to arbitrary cross-sections [8]. Abderahmane et al. [9] present a model the prestressed wave propagation that considers triaxial loading with arbitrary cross-sections, testing the superposition of the axial loading components.

Although Semi-Analytical methods are efficient for computing modes and dispersion curves, their use is limited to structures with relatively simple geometries [10], consequently to simple or canonical stress profiles. In this context, there is a need to fill in the gap by generic modeling and simulation of the influence of stress on wave propagation.

In this work, we present a generic numerical solver for ultrasonic wave propagation considering the effects of prestresses caused by structural loading. Relying on the differences in characteristic times and amplitudes between the structural loading and the ultrasonic actuators we can identify two problems: (1) a quasi-static nonlinear mechanical problem representing the structural displacement and (2) a linearized time-dependent wave problem representing the GW propagation. For each problem, we propose a relevant choice of numerical solver. For the first one, since classical Finite Elements Methods (FEM) suffers from shear-locking when thin structured are subjected to bending solicitation, we use the 3D Shell Finite Elements Method [11]. It allows us to overcome locking issues without simplifying assumptions on the mechanical model or the constitutive law. The wave propagation problem is solved using the 3D Spectral Finite Elements Method (SFEM) [12] in time-domain with a very low memory footprint [13]. Hence, the methods presented here can be used for any geometry subjected to a generic stress profile caused by structural loading and using any hyperelastic constitutive law. The combined numerical tools are validated using experimental data from the literature for an isotropic case with tensile loading. For illustration of bias induced by prestress, our method is also applied to a realistic pipe bending experiment with curved geometry and a complex stress profile.

This paper will be presented in four main sections. In section 2, we present the details of the mechanical modeling. In section 3, we validate our numerical tools based on another model and experimental data available in the literature. In section 4, we use the presented model and tools in a realistic scenario for highlighting the effect of prestresses. Finally in section 5, conclusions and perspectives are given.

2. MODELING OF PRESTRESSED WAVE PROPAGATION

In this section, we briefly introduce the nonlinear formulation for elastodynamics problems and the development made from this formulation to obtain a generic prestressed wave propagator. Our approach is to, by the nature of the problem, decompose the external forces into forces that causes the structural deformation and the ones that generates ultrasonic waves. We use the fact that these forces differ in time and amplitude to obtain two problems, one nonlinear quasi-static problem and one linearized wave propagation problem. In the presented work we achieve genericness by computing the prestress field from the nonlinear quasi-static mechanics problem and providing it as a structural displacement field to the wave propagator.

2.1 Nonlinear Mechanics

As a traditional approach in continuum mechanics [14, 15], we consider that the specimen to be modeled is initially on a stress-free reference configuration, which coordinate system is referred to as the Lagrangian referential. The deformed configuration, Eulerian referential, results from external forces acting in the specimen in its reference configuration. We use $\hat{x}$ and $\hat{\Omega}$, respectively, for the coordinates and the domain on the reference configuration. For the deformed configuration, we use x and Ω that may vary with time (see Fig. 1). We introduce the following relations between both domains

$$\boldsymbol{u}(\hat{\boldsymbol{x}},t) = \boldsymbol{x}(\hat{\boldsymbol{x}},t) - \hat{\boldsymbol{x}}, \quad \boldsymbol{x}(\hat{\boldsymbol{x}},t) = \boldsymbol{\phi}(\hat{\boldsymbol{x}},t)$$

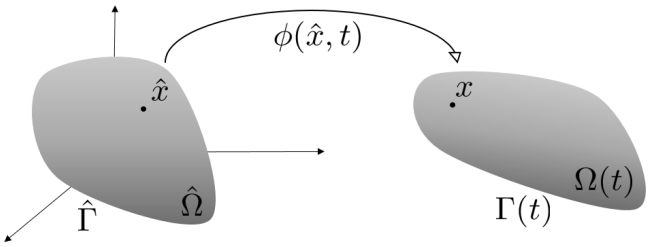

FIGURE 1: REFERENCE AND DEFORMED CONFIGURATIONS AND ITS ASSOCIATED NOTATION.

Considering the displacement field $\boldsymbol{u}$ and a body force $\boldsymbol{f}$, the equation of motion in continuum media over the domain Ω can be modeled by:

$$\rho\frac{\partial^2\boldsymbol{u}}{\partial t^2} - \boldsymbol{\nabla}_{\boldsymbol{x}}\cdot\boldsymbol{\sigma} = \rho\boldsymbol{f} \quad \text{in} \quad \Omega$$

where $\boldsymbol{\sigma}$ is the Cauchy stress tensor that relates strain and stresses through a constitutive law, $\boldsymbol{\nabla}_{\boldsymbol{x}}\cdot\boldsymbol{\sigma}$ is the divergent field of the stress tensor *w.r.t.* the deformed domain coordinates. Although for presenting the following formulations we consider only body forces, surface forces could be considered with further developments. We define the following space of admissible solutions

$$\mathcal{V}(\Omega) = \{v \in \mathrm{H}^1(\Omega)^3 \mid \boldsymbol{v} = 0 \text{ in } \Gamma^D\},$$

where Γ^D is the surface of the domain boundary assumed to be clamped. We can write the equivalent nonlinear problem in its weak formulation in the reference configuration $\hat{\Omega}$ as: find $u \in \mathcal{V}(\hat{\Omega})$ solution of

$$\forall w \in \mathcal{V}(\hat{\Omega}), \qquad \frac{\mathrm{d}^2}{\mathrm{d}t^2}m[u,w] + a(u)[w] = l[w]. \qquad (1)$$

where m, a and l are the operators related to the inertial, internal and external forces, respectively. Details on the operators are given in Appendix A. Note that in the following we use parenthesis to represent nonlinear dependency and square brackets to represent linear dependency.

2.2 Quasi-static and Linearized Wave Propagation problems

The nature of the forces acting in our system can be decoupled in time and amplitude. The structural loading can be considered quasi-static, not depending on time. The ultrasonic excitation is of high-frequency and low amplitude. We model, then, the external forces acting in the system decoupled as,

$$\boldsymbol{f}(\hat{\boldsymbol{x}}, t) = \boldsymbol{f}_0(\hat{\boldsymbol{x}}) + \delta\, \widetilde{\boldsymbol{f}}(\hat{\boldsymbol{x}}, t)$$

with $\delta \ll 1$. From this decomposition we propose the following Ansatz for the solution of problem (1)

$$\boldsymbol{u}(\hat{\boldsymbol{x}}, t) = \boldsymbol{u}_0(\hat{\boldsymbol{x}}) + \delta\, \widetilde{\boldsymbol{u}}(\hat{\boldsymbol{x}}, t) + O(\delta^2)$$

where $\boldsymbol{u}_0$ represents the static structural deformation and $\widetilde{\boldsymbol{u}}$ the high frequency ultrasonic perturbation. Inserting this decomposition of the solution in Eq. (1), we obtain relevant equations for u_0 and $\widetilde{u}$ by cancelling the zeroth order terms and first order terms *w.r.t.* δ and neglecting higher order terms.

By canceling the zeroth-order terms and first-order terms we derive the quasi-static and the wave propagation problems, respectively, that we detail and comment on in the following.

Quasi-Static Problem (zeroth-order terms). The first problem is the computation of the displacement field due to structural loading and can be written as: find $u_0 \in \mathcal{V}(\hat{\Omega})$ solution of

$$\forall w \in \mathcal{V}(\hat{\Omega}), \qquad a(u_0)[w] = l_0[w] \tag{2}$$

where l_0 is the right-hand side operator representing the structural loading. Details on the operators are given in Appendix A. This nonlinear static problem can be solved independently from the wave propagation problem and have as output the structural displacement field. When performing computations on thin structures, classical finite elements suffers from numerical locking, resulting in a stiffer structure and false convergence of the method. We use 3D Shell Finite elements that allow us to overcome this problem without the need for changing neither the formulation nor the constitutive law [11].

Wave Propagation Problem (first-order terms). The second problem obtained from cancelling first-order terms is the prestressed wave propagation problem: for all time $t > 0$, find $\widetilde{u}(t) \in \mathcal{V}(\hat{\Omega})$ solution of

$$\forall w \in \mathcal{V}(\hat{\Omega}), \qquad \frac{\mathrm{d}^2}{\mathrm{d}t^2} m[\widetilde{u}, w] + \mathrm{D}_u a(u_0)[\widetilde{u}, w] = \widetilde{l}[w] \tag{3}$$

where $\mathrm{D}_u a$ is the tangent stiffness operator around the deformed state u_0 and $\widetilde{l}$ is the right-hand side operator representing the ultrasonic excitation. When including surface forces the operator $\widetilde{l}$ depends also nonlinearly on u_0.

Additionally to being able to consider arbitrary stress profiles caused by deformation our formulation comprises the geometrical and constitutive nonlinearities in the tangent stiffness operator. Abderahmane points out in [9] that the geometrical term was usually neglected in previous works. Treyssède, in [5], considers that, for small quasi-static strains, the elasticity tensor does not change with prestresses, neglecting the constitutive nonlinearity. The constitutive nonlinearity is important for modeling quantitatively the effects of prestresses in wave propagation as shown in [16].

This weak formulation can be written in the stressed configuration Ω but the choice of stating the problem in the reference configuration $\hat{\Omega}$ becomes natural when we want to model ultrasonic wave propagation setups as most of the specifications are given in an stress-free state, such as transducer positions, sensibility and geometry. Material parameters and constitutive stress-strain relations are also defined in the reference configuration.

As the meshes for structural deformation computation and wave propagation are essentially different for their purposes, the structural displacement field must be interpolated over the wave propagation mesh. This interpolated field is used to compute the gradient of u_0 and as it is computed by element, the gradient tensor field is discontinuous. Each component of the gradient is then averaged at the elements' interfaces to be stored as a continuous tensor field.

Comparing the wave propagation problem presented here with classical elastodynamics problems we have as the main difference the tangent stiffness evaluated at a specific displacement field u_0 instead of the tangent stiffness operator evaluated at null displacement. As it can be seen with more details in the Appendix A, the tangent stiffness operator depends on the structural loading in a way that may cause stress-induced anisotropy and changes in the polarization of Lamb modes propagation [9]. Another important consideration is that this operator may be non-positive depending on the constitutive law used and the structural deformation, causing instabilities in the solver (i.e. divergence of the solution). One known case of such non-positivity is when we have structural buckling. For the presented realistic deformations and constitutive laws, this non-positivity was not present. Another important aspect to be considered is that the effects of prestresses on wave propagation cannot be considered only by changing the material parameters in classical elastodynamics solvers. Numerical wave propagation solvers usually use symmetries of the tangent stiffness operator that are not present in the prestressed case.

2.3 Constitutive Law and Calibration

The presented formulations for both problems are generic in terms of the geometry, of the structural loading and of the stress-strain relation appearing in the definition of the operators a and $\mathrm{D}_u a$. They depend on $\boldsymbol{\Sigma}$, the second Piola-Kirchhoff stress tensor (defined in Appendix A), and considering hyperelastic laws, this tensor can be derived from a hyperelastic potential W

$$\boldsymbol{\Sigma}(\boldsymbol{e}) = \mathrm{D}_{\boldsymbol{e}} W(\boldsymbol{e}), \tag{4}$$

where e is the Green-Lagrange tensor.

The choice of W and its characterizing parameters is complex and usually done by experimental efforts for each case. A constitutive law known and used in the acoustoelasticity community, that studies the effects of prestresses onto elastic wave propagation, is the Murnaghan's constitutive law. This law includes the third-order elastic constants l, m, and n to control the nonlinearity related to this acoustoelastic effect. Most of the time however,

for standardized industrial materials only Hooke's law parameters are available. It is the case, for instance, for composite materials potentially bearing stratified anisotropy. From this reduced – but commonly available – data it is still possible to enter the modeling framework presented in this communication. To do so, one only has to match the known Hooke's law with the tangent at null displacement of the second order Piola-Kirchhoff tensor $\boldsymbol{\Sigma}$. To give an illustrating example, let us consider an isotropic material with a constitutive law characterized by its Lamé parameters λ and μ. Denoting by $\boldsymbol{A}_{\lambda,\mu}$ the fourth-order tensor generating stress values from input strain tensors, namely $\boldsymbol{A}_{\lambda,\mu}\boldsymbol{\varepsilon} = \lambda \mathrm{tr}(\boldsymbol{\varepsilon})\mathbb{1} + 2\mu\boldsymbol{\varepsilon}$, then this simple (generic) calibration procedure reads

$$\mathrm{D}_{\boldsymbol{e}}\boldsymbol{\Sigma}\big|_{\boldsymbol{e}=0} = \boldsymbol{A}_{\lambda,\mu}.$$

Naturally, this relation suggests that the number of parameters in the nonlinear constitutive law matches the number of parameters in the Hooke's law. Applying this approach to the case of Compressible Neo Hookean, namely

$$\boldsymbol{\Sigma}^{CNH}(\boldsymbol{C}) = 2\alpha(\mathbb{1} - \boldsymbol{C}^{-1}) + 2\beta\sqrt{I_3}(\sqrt{I_3} - 1)\boldsymbol{C}^{-1},$$

with parameters α and β to be characterized, and where $\boldsymbol{C}$ is the right Cauchy-Green deformation tensor and $I_3 = \det \boldsymbol{C}$, we obtain the known relations

$$\alpha = \frac{\mu}{2}, \quad \beta = \frac{\lambda}{2}.$$

This calibration method can also be used for anisotropic cases, see for instance [17] in the case of transverse isotropic materials, typically representing unidirectional composites.

3. VALIDATION

To validate our model and simulation tools we apply them for modeling an experiment available in the literature [16]. In this experiment the authors applied tensile forces to an 6061-T6 aluminium plate and measured the differences in guided waves velocities caused by the prestresses. The tensile forces were applied in 11 steps from 0MPa to 57.5MPa.

First, we compute the deformation of the aluminium plate for each tensile solicitation. The surface forces that represents the tensile solicitation is added directly at Eq. (2) as a surface integral operator. When these forces are considered before the linearization presented in Sec. 2.2 it adds a surface term (integral over the structural solicitation domain) in the wave propagation problem. As, for the validation configuration, the waves do not travel up to these boundaries, we neglect this term. We use the proposed constitutive law (Murnaghan's [18]) and proposed material parameters (Table 1, including third-order elastic constants). Material parameters for 6061-T6 aluminium can be found in the literature [19], but as the third-order elastic constants vary considerably from one specimen to another, we used the fitted parameters to the experimental results, available in [16].

Each computed structural displacement field, for each level of force, was interpolated over the wave propagation mesh and given as input to the wave propagator to compute the wavefield generated by the transducers. The transducers were added directly in the formulation (3) as a surface operator. Further developments must be made in this surface operator to proper modeling of the effects of the deformation on the transducer although it will not affect the wave velocities.

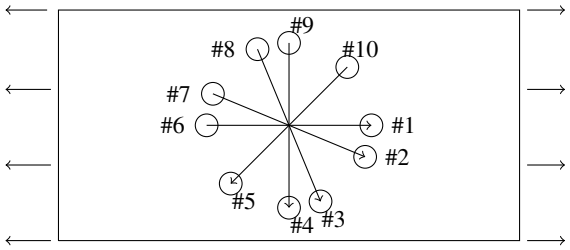

FIGURE 2: EXPERIMENTAL CONFIGURATION: ALUMINIUM PLATE SUBJECTED TO TENSILE FORCES UP TO 57.5MPa. CONSIDERED PITCH-CATCH PAIRS ARE DEPICTED.

Our analysis is done for the S0 Lamb wave mode for a frequency of 250kHz as it can be easily extracted from the signal. The changes in S0 mode in-axis velocity for different force levels are presented in Fig. 3. We plot our results (Model FE), their experimental results and proposed model.

The velocity measurements obtained by the authors were done by zero-crossing marking, but the specific zero-crossing was not given. As the Lamb waves are dispersive, the choice of the zero-crossing influences the measured velocity, for that reason we plot a range of solutions for different choices. Although the S0 mode is not much dispersive, its influence is relevant for the presented measurements and travelled distances.

TABLE 1: ALUMINIUM MATERIAL PARAMETERS USED FOR OUR SIMULATION. SECOND AND THIRD ORDER ELASTIC CONSTANTS. [16]

Parameter	Value
Density	2700 kg/m^3
λ	54.308 GPa
μ	27.174 GPa
l	−181 GPa
m	−289 GPa
n	−336 GPa

The axial prestresses also causes the material to become slightly anisotropic, hence we compare their change in wave velocity for different angles of propagation by simulation. The transducer positions and the measured direction velocities are depicted in Fig. 2. For a fixed stress level of 57.5MPa we plot (Fig. 4) the change in velocity for different propagation angles (where 90º is the loading axis). Our results are coherent with the model presented in [16] and the experimental results can be reproduced using our approach.

4. NUMERICAL ILLUSTRATION

During a four-point bending test a given specimen is supported in two locations and bending forces are applied in two different locations. This bending test is usually used for fatigue test in welded piped.

We model and simulate a four-point bending test on a steel pipe inspired by [20]. Bending forces of 220kN was used to

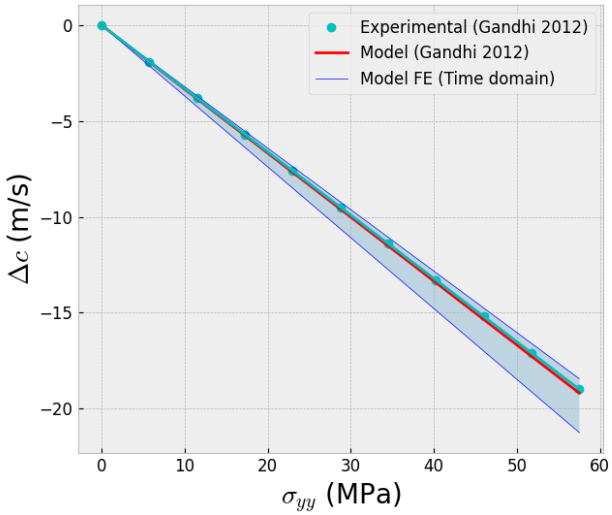

FIGURE 3: VELOCITY CHANGE (S0 MODE) DUE TO PRESTRESSES WITH FITTED PARAMETERS.

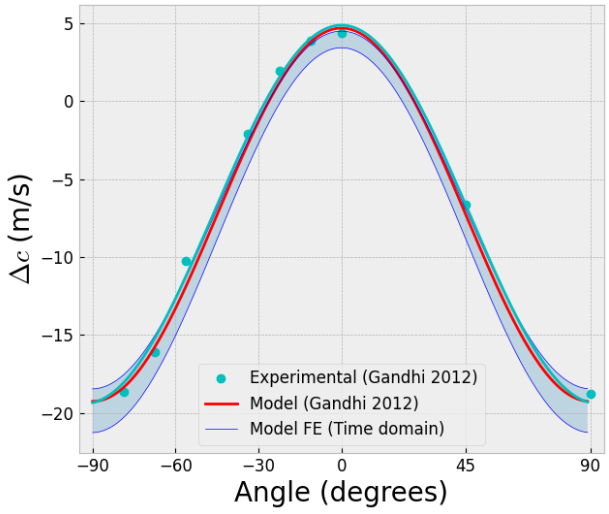

FIGURE 4: VELOCITY CHANGE (S0 MODE) DUE TO PRESTRESSES (57.5MPa) RELATIVE TO THE ANGLE OF PROPAGATION WITH FITTED MATERIAL PARAMETERS.

TABLE 2: QUASI STATIC SIMULATION CHARACTERISTICS

Dimensions	2.94m, Ø 0.1973m 8mm thick
Degrees of Freedom	300k
Method	3D Shell FE
Memory Peak	4.7GB
Runtime	4 minutes

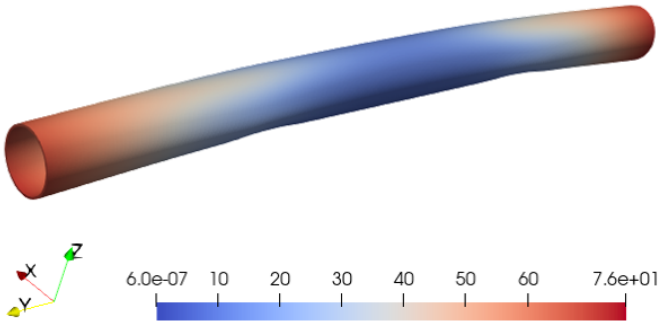

FIGURE 5: THE DISPLACEMENT FIELD (IN *mm*) COMPUTED FOR THE APPLIED BENDING FORCES.

induce deformation and internal stresses. Details of the model and the quasi-static computation can be found at Table 2 and the results can be seen at Fig. 5.

The displacement field computed by the 3D Shell FE is given as input for the wave propagator. A radial ultrasonic transducer was modeled to excite a 80kHz perturbation close to one of the pipe extremities. The displacement field was extracted close to the other extremity. Details on the wave propagation simulation are given in Table 3. A snapshot is presented at Fig 6. Note that the low-memory peak in Table 3 is due to a non-assembled implementation of the tangent stiffness operator. Using the presented methods, extensions can be made such as the implementation of several sensors and excitation models and transducer models.

To highlight the importance of considering the prestresses, we use this same experimental setup. The numerical setup is depicted in Fig. 7. We ran three different simulations with the same excitation and extraction points. The extracted signals are:

- S: non deformed pipe (considered as baseline; no defect).
- S_p: deformed pipe (no defect).
- S_d: pipe with defect (no prestresses).

Considering S as the baseline, we perform baseline subtraction to detect anomalies. The crack was modeled as disconnected elements. Figure 8 shows the differences between the extracted signals. The effects of the prestress in this case are of greater importance when compared to a crack localized close to the extraction point.

5. CONCLUSIONS AND PERSPECTIVES

In the context of Environmental and Operational conditions in Structural Health Monitoring, we present a model and associated numerical tools for wave propagation in deformed/prestressed media. The presented model can be implemented for arbitrary non-buckling deformations and arbitrary hyperelastic laws. Geometrical and constitutive nonlinearities are not neglected. The modeling shows that classic available solvers for elastodynamics cannot represent prestressed wave propagation as they use some symmetries of the tangent stiffness operator that are lost for the prestressed case. The model was validated against experimental results for the isotropic case. A numerical illustration was presented for a case with curved geometry and

TABLE 3: WAVE PROPAGATION SIMULATION CHARACTERISTICS

Degrees of Freedom	12M
Timesteps	5.1k
Excitation Freq.	80kHz
Method	Time domain (Explicit Leap Frog) SFEM
Memory Peak	2.8GB
Runtime	20 minutes

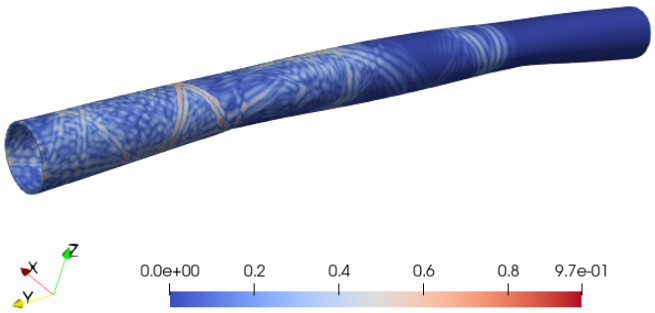

FIGURE 6: A SNAPSHOT OF THE WAVE PROPAGATION (IN μm) SIMULATED ON A STEEL PIPE SUBJECTED TO BENDING FORCES.

non-canonical prestresses. The presented method can be applied to a wide variety of industrial cases and it is capable of running large simulations even in standard workstations.

Advances must be made on the mechanical modeling of prestressed wave propagation for different kinds of materials. The choice of proper constitutive law and material parameters that take into account the wave propagation nonlinearities is not straightforward. These advances in hyperelastic laws that models the prestressed behavior can be straightforwardly implemented with our model and numerical tools. Anisotropy can be also considered, such as the transverse isotropy case of carbon fiber reinforced polymer (CFRP) layers, an important composite material present in aeronautical structures.

As a specialized code is needed for this type of wave propagation, efforts on simplifications may be made for retrieving the lost symmetries in the tangent stiffness operator so classical numerical solvers for mechanics could take advantage of these formulations. Future work includes the integration of the presented methods in the CIVA SHM software with its provided transducer models and user interface [21] and the use of this direct wave propagation solver in inversion loops for reconstructing structural loads and deformations. Further development and analysis can be made regarding the linearized surface terms.

ACKNOWLEDGMENTS

This research was funded by the following project: "GW4SHM" (gw4shm.eu) project from the European Union's Horizon 2020 Research and Innovation program under the Marie Skłodowska-Curie, grant number 860104.

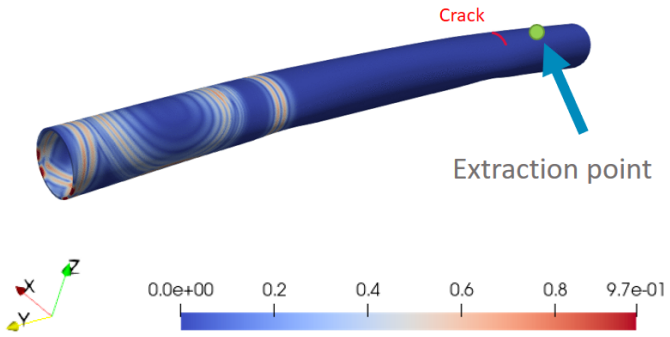

FIGURE 7: CONFIGURATION OF THE SIMULATION USED FOR PRESTRESSES EVALUATION. DATA IN (IN μm).

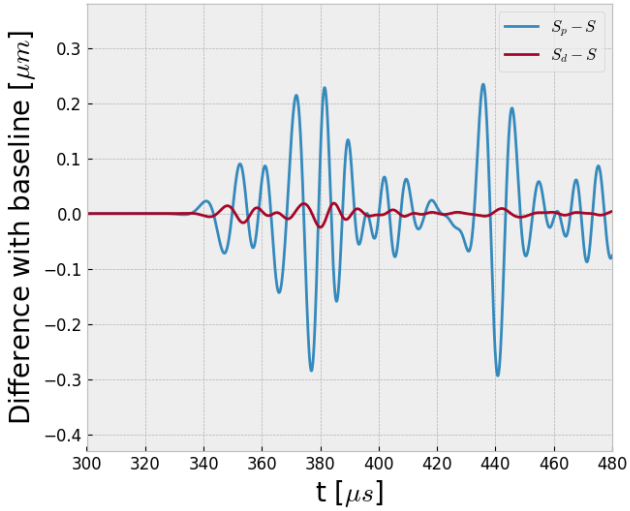

FIGURE 8: BASELINE SUBTRACTION WHEN CONSIDERING THE PRESENCE OF A CRACK VERSUS THE PRESENCE OF PRESTRESSES. COMPONENT Y IS PRESENTED.

REFERENCES

[1] Mitra, Mira and Gopalakrishnan, S. "Guided wave based structural health monitoring: A review." *Smart Materials and Structures* Vol. 25 No. 5 (2016): p. 053001. DOI 10.1088/0964-1726/25/5/053001.

[2] Ricci, Fabrizio, Monaco, Ernesto, Boffa, Natalino D., Maio, Leandro and Memmolo, Vittorio. "Guided waves for structural health monitoring in composites: A review and implementation strategies." *Progress in Aerospace Sciences* Vol. 129 (2022): p. 100790. DOI 10.1016/j.paerosci.2021.100790.

[3] Gorgin, Rahim, Luo, Ying and Wu, Zhanjun. "Environmental and operational conditions effects on Lamb wave based structural health monitoring systems: A review." *Ultrasonics* (2020): p. 106114Publisher: Elsevier.

[4] Michaels, Jennifer, Lee, Sang-Jun, Chen, Xin, Shi, Fan and Michaels, Thomas. *Understanding and Exploiting Applied Loads for Guided Wave Structural Health Monitoring*

(2011). DOI 10.13140/RG.2.1.2795.6648.

[5] Treyssède, Fabien, Frikha, Ahmed and Cartraud, Patrice. "Mechanical modeling of helical structures accounting for translational invariance. Part 2 : Guided wave propagation under axial loads." *International Journal of Solids and Structures* Vol. 50 No. 9 (2013): pp. 1383–1393. DOI 10.1016/j.ijsolstr.2013.01.006.

[6] Loveday, Philip W. and Wilcox, Paul D. "Guided wave propagation as a measure of axial loads in rails." *Health Monitoring of Structural and Biological Systems 2010*, Vol. 7650: p. 765023. 2010. International Society for Optics and Photonics. DOI 10.1117/12.847531.

[7] Shi, Fan, Michaels, Jennifer E. and Lee, Sang Jun. "In situ estimation of applied biaxial loads with Lamb waves." *The Journal of the Acoustical Society of America* Vol. 133 No. 2 (2013): pp. 677–687. DOI 10.1121/1.4773867. Publisher: Acoustical Society of America.

[8] Wu, Zhanjun, Yang, Zhengyan, Zhang, Jiaqi, Liu, Kehai, Jiang, Youqiang and Zhou, Kai. "Acoustoelastic guided wave propagation in axial stressed arbitrary cross-section." *Smart Materials and Structures* Vol. 28. DOI 10.1088/1361-665X/aadb6e.

[9] Abderahmane, Abdellahi, Lhémery, Alain and Daniel, Laurent. "Effects of multiaxial pre-stress on Lamb and shear horizontal guided waves." *The Journal of the Acoustical Society of America* Vol. 149 No. 3 (2021): pp. 1724–1736. DOI 10.1121/10.0003630. Publisher: Acoustical Society of America.

[10] Willberg, Christian, Duczek, Sascha, Vivar-Perez, Juan M. and Ahmad, Zair A. B. "Simulation Methods for Guided Wave-Based Structural Health Monitoring: A Review." *Applied Mechanics Reviews* Vol. 67 No. 1 (2015): p. 010803. DOI 10.1115/1.4029539.

[11] Chapelle, Dominique and Bathe, Klaus-Jurgen. *The Finite Element Analysis of Shells - Fundamentals*, 2nd ed. Computational Fluid and Solid Mechanics, Springer-Verlag, Berlin Heidelberg (2011). DOI 10.1007/978-3-642-16408-8.

[12] Cohen, Gary C. *Higher-order numerical methods for transient wave equations*, softcover reprint of the hardcover 1st edition ed. Scientific computation, Springer-Verlag, Berlin Heidelberg (2002).

[13] Imperiale, Alexandre and Demaldent, Edouard. "A macro-element strategy based upon spectral finite elements and mortar elements for transient wave propagation modeling. Application to ultrasonic testing of laminate composite materials." *International Journal for Numerical Methods in Engineering* Vol. 119 No. 10 (2019): pp. 964–990. Publisher: Wiley Online Library.

[14] Lopez-Pamies, Oscar. *The Mechanics of Solids: A Continuum Perspective*. Editions de l'Ecole Polytechnique (2021).

[15] Bonet, Javier and Wood, Richard D. *Nonlinear continuum mechanics for finite element analysis*. Cambridge University Press, Cambridge ; New York, NY, USA (1997).

[16] Gandhi, Navneet, Michaels, Jennifer E and Lee, Sang Jun. "Acoustoelastic Lamb wave propagation in biaxially stressed plates." *The Journal of the Acoustical Society of America* Vol. 132 No. 3 (2012): pp. 1284–1293. Publisher: Acoustical Society of America.

[17] Bonet, Javier and Burton, A. J. "A simple orthotropic, transversely isotropic hyperelastic constitutive equation for large strain computations." *Computer methods in applied mechanics and engineering* Vol. 162 No. 1-4 (1998): pp. 151–164. Publisher: Elsevier.

[18] Hughes, Darrell S. and Kelly, John L. "Second-Order Elastic Deformation of Solids." *Physical Review* Vol. 92 No. 5 (1953): pp. 1145–1149. DOI 10.1103/PhysRev.92.1145. Publisher: American Physical Society.

[19] Asay, James R. and Guenther, Arthur H. "Ultrasonic Studies of 1060 and 6061-T6 Aluminum." *Journal of Applied Physics* Vol. 38 No. 10 (1967): pp. 4086–4088. DOI 10.1063/1.1709077. Publisher: American Institute of Physics.

[20] Tschöke, Kilian, Weihnacht, Bianca, Schulze, Eberhard, Gaul, Tobias, Schubert, Lars and Neubeck, Robert. "Determination of Defect Sizes with the help of Structural-Health-Monitoring Methods based on Guided Waves." *2017-12*. 2017.

[21] "CIVA SHM - Extende." https://www.extende.com/structural-health-monitoring-with-civa.

[22] Komatitsch, Dimitri and Vilotte, Jean-Pierre. "The spectral element method: An efficient tool to simulate the seismic response of 2D and 3D geological structures." *Bulletin of the Seismological Society of America* Vol. 88 No. 2 (1998): pp. 368–392.

[23] Ostachowicz, W. M. (ed.). *Guided waves in structures for SHM: the time-domain spectral element method*. Wiley, Chichester, West Sussex ; Hoboken, NJ (2012).

[24] Carrascal-Manzanares, Carlos, Imperiale, Alexandre, Rougeron, Gilles, Bergeaud, Vincent and Lacassagne, Lionel. "A fast implementation of a spectral finite elements method on CPU and GPU applied to ultrasound propagation." *International Conference on Parallel Computing*. 2017. IOS Press, Bologna, Italy.

[25] Maday, Yvon and Patera, Anthony T. *Spectral element methods for the incompressible Navier-Stokes equations* (1989). State-of-the-art surveys on computational mechanics. New York. Pages: 71-143.

APPENDIX A. DEFINITION OF THE OPERATORS

We specify here the operators for the presented weak formulations. First, we recall the definitions of the following tensors

$$\boldsymbol{F}(\hat{\boldsymbol{x}},t) = \boldsymbol{\nabla}_{\hat{\boldsymbol{x}}}\,\boldsymbol{\phi}(\hat{\boldsymbol{x}},t), \quad \boldsymbol{C} = \boldsymbol{F}^{\intercal}\boldsymbol{F}, \quad J = \det \boldsymbol{F},$$

$$\boldsymbol{e}(\boldsymbol{u}) = \frac{1}{2}(\boldsymbol{C} - 1) \quad \text{and} \quad \boldsymbol{\Sigma}(\boldsymbol{e}) = J\boldsymbol{F}^{-1}\boldsymbol{\sigma}\,\boldsymbol{F}^{-\intercal}.$$

The operators for the classical nonlinear elastodynamics are:

$$m[u,w] = \int_{\hat{\Omega}} \widehat{\rho}\,\boldsymbol{u}\cdot\boldsymbol{w}\,\mathrm{d}\hat{\Omega},$$

$$a(u)[w] = \int_{\hat{\Omega}} \boldsymbol{\Sigma}(\boldsymbol{e}(\boldsymbol{u})) : \mathrm{D}_{\boldsymbol{u}}\,\boldsymbol{e}(\boldsymbol{u})[\boldsymbol{w}]\,\mathrm{d}\hat{\Omega},$$

$$l[w] = \int_{\hat{\Omega}} \widehat{\rho}\boldsymbol{f}\cdot\boldsymbol{w}\,\mathrm{d}\hat{\Omega},$$

where $\widehat{\rho} = J\rho$. For the Quasi-Static problem we have

$$l_0[w] = \int_{\hat{\Omega}} \widehat{\rho} \boldsymbol{f}_0 \cdot \boldsymbol{w} \, \mathrm{d}\hat{\Omega}.$$

For the Wave Propagation problem we have

$$\mathrm{D}_u a(u_0)[\widetilde{u}, w] = \int_{\hat{\Omega}} \mathrm{D}_{\boldsymbol{u}} \, \boldsymbol{e}(\boldsymbol{u}_0)[\widetilde{u}] : \mathrm{D}_{\boldsymbol{e}} \boldsymbol{\Sigma}(\boldsymbol{e}(\boldsymbol{u}_0)) : \mathrm{D}_{\boldsymbol{u}} \, \boldsymbol{e}(\boldsymbol{u}_0)[\boldsymbol{w}] \, \mathrm{d}\hat{\Omega} + \int_{\hat{\Omega}} \boldsymbol{\Sigma}(\boldsymbol{e}(\boldsymbol{u}_0)) : \mathrm{D}^2_u \boldsymbol{e}[\widetilde{\boldsymbol{u}}, \boldsymbol{w}] \, \mathrm{d}\hat{\Omega} \quad \text{and}$$

$$\widetilde{l}[w] = \int_{\hat{\Omega}} \widehat{\rho} \widetilde{\boldsymbol{f}} \cdot \boldsymbol{w} \, \mathrm{d}\hat{\Omega},$$

where the second derivative of the Green-Lagrange strain tensor is

$$\mathrm{D}^2_u \boldsymbol{e}[\widetilde{\boldsymbol{u}}, \boldsymbol{w}] = \frac{1}{2}\Big(\boldsymbol{\nabla}^{\intercal}_{\hat{\boldsymbol{x}}} \boldsymbol{w} \, \boldsymbol{\nabla}_{\hat{\boldsymbol{x}}} \widetilde{\boldsymbol{u}} + \boldsymbol{\nabla}^{\intercal}_{\hat{\boldsymbol{x}}} \widetilde{\boldsymbol{u}} \, \boldsymbol{\nabla}_{\hat{\boldsymbol{x}}} \boldsymbol{w} \Big).$$

APPENDIX B. CONSTITUTIVE LAWS

We present here some hyperelastic potentials for isotropic cases that were calibrated with the Hooke's Law. Third-order elastic constants l, m, and n are included for the Murnaghan's law. Isotropic Hyperelastic laws depend uniquely on the three first Right Cauchy-Green tensor invariants

$$I_1 = \mathrm{tr}(\boldsymbol{C}), \qquad I_2 = \frac{1}{2}\Big(\mathrm{tr}(\boldsymbol{C})^2 - \mathrm{tr}(\boldsymbol{C}^{\intercal}\boldsymbol{C}) \Big), \qquad I_3 = \det \boldsymbol{C}.$$

The hyperelastic potential of Saint-Venant-Kichhoff (SVK), Compressible Neo Hookean (CNH) and Murnaghan's (MUR) constitutive laws are, respectively

$$W^{\mathrm{SVK}} = \frac{(\lambda + 2\mu)}{8} I_1^2 - \frac{(3\lambda + 2\mu)}{4} I_1 - \frac{\mu}{2} I_2 + \frac{(9\lambda + 6\mu)}{8},$$

$$W^{\mathrm{CNH}} = \frac{\lambda}{2}(\sqrt{I_3} - 1)^2 + \frac{\mu}{2}(I_1 - 3 - \log(I_3)) \quad \text{and}$$

$$W^{MUR} = \frac{\lambda + 2\mu}{8}(I_1 - 3)^2 - \frac{\mu}{2}(3 - 2I_1 + I_2) + \frac{l + 2m}{24}(I_1 - 3)^3 - \frac{m}{4}(9I_1 - 3I_2 - 2I_1^2 + I_1 I_2 - 9) - \frac{n}{8}(I_1 - I_2 + I_3 - 1).$$